SYNTHESIS AND DEVELOPMENT OF Mg-SUBSTITUTED HYDROXYAPATITE OBTAINED FROM NATURAL SOURCES

Diana-Elena RADULESCU[1], Bogdan Stefan VASILE[2], Ionela Andreea NEACSU[1], Adrian Vasile SURDU[1], Alexandra Catalina BIRCA[2] Roxana Doina TRUSCA[1], Ecaterina ANDRONESCU[1, 3, 4,*]

Over the last decade, the necessity to improve osseous tissue regeneration has gained great interest, focusing on the treatment of damaged tissues due to accidents or orthopedic disorders. Further, bone regeneration is mostly influenced by the dimensions of the affected tissue which could lead to additional surgeries. The latest studies focused on the development of novel materials that could improve bone healing without affecting the surrounding tissues, thus avoiding any additional treatments. As hydroxyapatite is the most used material in bone tissue engineering, researchers focused on developing new synthesis methods with the aid of biogenic sources. In this regard, this study focused on the synthesis of hydroxyapatite materials using mussel shells and eggshells as CaO sources, in which the Ca^{2+} ions were further substituted with Mg^{2+} ions in different molar concentrations (1%, 3%, and 5% respectively). The morpho-structural and biological characteristics of the obtained powders were investigated to confirm their applicability to the biomedical field. With the aid of XRD, SEM, and FT-IR analyses, the successful synthesis of hydroxyapatite and incorporation of doping ions were confirmed. Moreover, the obtained samples showed good biological activity on MC3T3-E1 osteoblast cells. Considering these aspects, it could be assumed that both substituted and unsubstituted powders are suitable for further application in bone tissue engineering.

Keywords: hydroxyapatite, biogenic calcium sources, Mg^{2+} doping, bone tissue engineering

1. Introduction

Bone tissue engineering has been widely investigated to develop the ideal solutions for the enhancement of osseous regeneration without affecting the human body. In this regard, nanomaterials, especially calcium phosphates, have been

[1] Department of Science and Engineering of Oxide Materials and Nanomaterials, Faculty of Chemical Engineering and Biotechnologies, National University of Science and Technology POLITEHNICA Bucharest, Romania, e-mail: radulescu.diana95@gmail.com

[2] Advanced Research Center for Innovative Materials, Products and Processes, National University of Science and Technology POLITEHNICA Bucharest, Romania, Bogdan.vasile@upb.ro

[3] Academy of Romanian Scientists, Ilfov, Bucharest, Romania

[4] National Research Center for Micro and Nanomaterials, Faculty of Applied Chemistry and Materials Science, National University of Science and Technology POLITEHNICA Bucharest, Romania

*Corresponding authors: ecaterina.andronescu@upb.ro

preferred due to their excellent biocompatibility, osteoinductivity, and osteoconductivity. Hydroxyapatite (HAp) with the chemical formula $Ca_{10}(PO_4)_6(OH)_2$, is the main mineral component found in osseous tissues. This material is chosen for numerous applications, such as dental, maxillofacial, and orthopedic treatments for the reconstruction of affected tissues due to its biological activity. Nevertheless, its poor mechanical characteristics such as low fracture toughness, absorbability, and instability limit its effectiveness in load-bearing applications or surface coatings of implants. The biological behavior of HAp is highly influenced by their phase and chemical composition, pore dimensions, and size, but also microstructure. To solve this issue, researchers focused on various approaches to improve its mechanical properties, such as dopants incorporation into the chemical structure of the material [1]. The incorporation of various elements into the HAp structure has been studied extensively due to its flexibility in incorporating various doping ions. The success of an in vivo implant can be highly influenced by specific doping ions, essential for protein aggregation. Considering these aspects, Ca^{2+} ions in the HAp crystal lattice could be substituted by numerous ions such as Ag^{+}, Al^{3+}, Ni^{2+}, Zn^{2+}, Ce^{3+}, Mg^{2+}, Sr^{2+}, Na^{+}, Cu^{2+}, and so on. This modification is generated by the strong ion exchange capacity and crystal structure, which is composed of Ca^{2+}, $(PO_4)^{3-}$, and OH^{-} [2]. All these ions present the ability to enhance the mechanical properties of the material. In this direction, Mg^{2+} has been preferred for the substitution into the HAp lattice due to its additional biological properties. Sebastiammal [3] mentioned that Mg^{2+} incorporation into the chemical structure led to a decrease in bone fragility, reducing the risk of the apparition of osteoporosis. Moreover, these ions were proven to have the capacity to increase new blood vessel development through the stimulation of endothelium. Ţălu et al. [4] also reported that its incorporation improved bone density, avoiding the appearance of fractures. Furthermore, Helen et al. [5] mentioned that Mg doping showed substantial development in osteoblast activity. This ionic substitution in HAp presents the capacity to improve the lattice parameters, surface charge, morphology, and crystallinity. All these modifications highly influence thermal stability, solubility, mechanical properties, osteogenic potential, and bioactivity.

On the other hand, numerous researchers focused on the synthesis of HAp from biogenic sources [6]. In comparison to the HAp synthesized from chemical routes, natural-based HAp exhibited promising results considering the bioactivity of the material. The developed materials show superior biocompatibility and an enhanced inflammatory repair system. In this regard, seashells, eggshells, or fish bones are natural sources used for HAp production [7]. Further, HAp obtained from biogenic sources is not only preferred due to its bioactivity but also due to its non-toxicity, low costs, and compatibility with numerous applications [8]. Compared with chemically synthesized HAp, natural-based HAp is non-stoichiometric and can retain the pore structure and traces elements such as Zn^{2+}, Na^{+}, K^{+}, Mg^{2+}, Si^{2+},

and F^-, which is like the chemical composition of osseous tissues [9]. The preparation of HAp from biogenic sources is performed through various methods, involving the co-precipitation method, dry method, hydrothermal method, and sol-gel method. The hydrothermal technique is extensively selected from the aforementioned synthesis methods for its capacity to obtain homogeneous and crystalline products. Microwave-assisted hydrothermal synthesis usually produces HAp with uniform particle size distribution and ample porosity [10]. From all the synthesis methods mentioned above, the hydrothermal method has been extensively applied to obtain materials with tunable sizes, structures, and morphologies. However, this technique requires a long reaction time. Liu et al. mentioned that the microwave-assisted method could intensely reduce reaction time due to its thermal and non-thermal effects. Further, this method combined the advantages of both microwave and hydrothermal methods, accelerating the completion of the reaction in a sealed system [11]. Considering HAp synthesis, microwave radiation's energy can accelerate the HAp production rate via the direct interaction of electromagnetic microwave radiation with the polar solvent molecules [12].

Considering all these aspects, there are few studies presented for the synthesis of ion-substituted HAp using biogenic calcium sources, normally considered biowaste. In the last few years, researchers focused on the substitution of natural-based HAp to investigate the effects of both mechanical and biological properties of the developed materials. Moreover, the combined effect between the CaO source and doping ions has not yet been fully demonstrated. On the other hand, the development of ion-substituted HAp, obtained from biogenic sources presents great potential for the microwave-assisted hydrothermal method. This study aims to synthesize HAp by using biowastes, such as eggshells and mussel shells, as CaO sources. The obtained samples were substituted with Mg^{2+} ions in different concentrations. Furthermore, the developed materials were examined considering their morpho-structural features and biological activity, respectively the cellular viability.

2. Materials and Methods

2.1. Materials

For the synthesis of unsubstituted and Mg-substituted HAp, the following precursors were used: $(NH_4)_2HPO_4$ (98%), $MgCl_2 \cdot 6H_2O$ (99%) from Sigma–Aldrich, Saint Luis, MO, USA, and distilled water. Further, to obtain CaO, eggshells, and mussel shells were received from a local restaurant. Additionally, fetal bovine serum, DMEM medium (Sigma-Aldrich, Saint Luis, MO, USA), and XTT reagent (2,3-Bis-(2-Methoxy-4-Nitro-5-Sulfophenyl)-2H-Tetrazolium-5-Carboxanilide) (Thermo Fischer Scientific, Waltham, MA, USA) were used for the XTT Cell Viability Assay.

2.2. Unsubstituted and Mg-Substituted Hydroxyapatite Synthesis Method from Biogenic Sources

The procured mussel shells were cleansed with boiled water for the removal of impurities that were attached to the shells. For the next step, the shells were washed with distilled water and immersed into the ultrasonic bath to eliminate any other residues left. After washing, the mussel shells were dried in the oven at 60℃ for 48 h and followed by manual grinding in a mortar until a fine powder was obtained. The resulting powder was heat treated at 1000℃ for 3 h. Considering the eggshells, their membrane was firstly removed through their immersion in an HCl 0.5 M solution. After the organic parts of eggshells were removed, the same process applied to mussel shells was used to obtain CaO precursor. HAp synthesis was accomplished with the aid of the co-precipitation method followed by the microwave-assisted hydrothermal maturation process with the aid of the synthWAVE equipment (Milestone Srl, Sorisole, Bergamo, Italy). Firstly, a solution of $(NH_4)_2HPO_4$ was prepared by dissolving 11.04 g in 200 mL of distilled water, while 7.8 g of CaO was dispersed in 200 mL of distilled water. For the experiments, both CaO obtained from eggshells and mussel shells were used. The phosphate solution was added dropwise into the Ca^{2+} dispersion under magnetic stirring at room temperature. Throughout the precipitation, the pH was maintained around 9-10. After it reached the desired pH value, the mixture was poured into the vessel of microwave-assisted equipment and subjected to hydrothermal maturation. The microwave-assisted hydrothermal synthesis method was performed in specific conditions, with an initial pressure of 2 bars; in 2 min the temperature increased to 120°C and remained constant for the following 10 min. After maturation, the resulting precipitates were filtered, washed with distilled water until reaching neutral pH, and then dried in the oven at 60 ℃ for 48 h. For the Mg-substituted HAp, the synthesis process was similar to unsubstituted HAp synthesis. The only particularity was the addition of the $MgCl_2 \cdot 6H_2O$ precursor. To obtain Mg-substituted HAp, various quantities of precursors were used corresponding to different Ca^{2+} substitution molar ratios (1%, 3%, and 5%). Separate solutions of corresponding precursors were introduced into the CaO dispersion, under magnetic stirring before adding the phosphate solution. All obtained solutions followed the same process of hydrothermal maturation in the microwave field. Considering the biogenic source and doping ion, the samples were labeled as specified in Table 1.

Table 1

Codification of the obtained samples (1%, 3%, and 5% representing the concentrations of the doping ion).

Source	Code
Eggshell (C)	HAp_C
	HAp_Mg_1_C

	HAp_Mg_3_C
	HAp_Mg_5_C
Mussel shells (S)	HAp_S
	HAp_Mg_1_S
	HAp_Mg_3_S
	HAp_Mg_5_S

2.3. Characterization Methods

2.3.1. X-ray Diffraction (XRD)

The crystallinity and crystal parameters of the synthesized samples were analyzed using an Empyrean diffractometer with CuKα radiation provided by PANalytical (PANalytical, Almelo, The Netherlands). The obtained patterns were registered between the 2θ angle values of 20 and 80°, with a 0.0256° step size and 1 s time per step. In addition, the diffractograms were fitted with the aid of the Rietveld refinement algorithm using HighScore Plus software (version 3.0, PANalytical, Almelo, The Netherlands) and the ICDD PDF4+ 2022 database. For the refinement of the procured diffractograms, goodness of fit < 4 was considered suitable to determine the crystallinity and structural parameters of each sample. The average crystallite size was determined with the use of the Scherrer equation.

2.3.2. Scanning Electron Microscopy (SEM)

The morphology of the obtained samples was investigated using a QUANTA INSPECT F50 scanning electron microscope (Thermo Fisher, Eindhoven, The Netherlands). The microscope was equipped with a field electron emission gun (FEG), with a resolution of 1.2 nm, and an EDS (Energy Dispersive Spectroscopy) detector, with a resolution at MnK of 133 eV. The powder samples were fixed on a carbon-bearing slide and introduced in an analysis chamber.

2.3.3. Fourier-Transform Infrared Spectroscopy (FT-IR)

The functional groups present in the obtained materials were assessed through the acquisition of IR spectra. In this regard, a Thermo Scientific Nicolet iS50 (Thermo Fischer Scientific, Waltham, MA, USA) spectrometer was used. The acquisitions were made at room temperature, with a resolution of 4 cm^{-1} resolution, 64 scans for each sample, at the 4000–400 cm^{-1} wavenumber range. The equipment recorded the data obtained by connecting the spectrometer to a data collection and processing device using the Omnic work program. (Thermo Nicolet, Version 8.2).

2.3.4. Biological Evaluation

Considering the biological activity of the synthesized substituted and unsubstituted HAp samples, the biocompatibility was examined using XTT reagent (2,3-Bis-(2-Methoxy-4-Nitro-5-Sulfophenyl)-2H-Tetrazolium-5-Carboxanilide) according with the manufacturer procedure (CyQUANT™ XTT Cell Viability Assay Kit, Thermo Fischer Scientific, Waltham, MA, USA). In the assay kit, it is

included also the Electron Coupling Reagent and XTT reagent. The XTT reagent is a tetrazolium-based compound sensitive to the cellular redox potential. The water-soluble XTT compound is converted by the actively viable cells into an orange-coloured formazan product. The consistency and sensitivity of the analysis were substantially amplified when using the Electron Coupling Reagent. The MC3T3 cell line was grown in DMEM medium (Sigma-Aldrich, Saint Luis, MO, USA) supplemented with 1% antibiotics (penicillin and streptomycin) and 10% fetal bovine serum, (Sigma-Aldrich, Saint Luis, MO, USA), which was changed twice a week. The cells were put in 96-well plates, at a density of 3000 cells/well in the presence of substituted and unsubstituted HA samples for 24h, and 48 h. Also, the control samples were only the cells cultivated in identical conditions, but without the synthesized samples. Subsequently, 70 μL of XTT solution was added to the cells, followed by incubation at 37°C for 4 h. After energetic homogenization of formazan crystals, the absorbance was read at 450 nm using a spectrophotometer.

3. Results and Discussion

3.1. Results

3.1.1. X-ray Diffraction (XRD)

In Fig. 1 the diffraction patterns of the powders obtained through the co-precipitation method followed by a microwave-assisted hydrothermal maturation process are presented. The results indicate the successful synthesis of HAp using eggshells and mussel shells as CaO precursors. Considering the type of biogenic source, the unsubstituted sample obtained from eggshells confirmed HAp synthesis (ICDD PDF4+ 96-900-2215), with a reduced quantity of $Ca(OH)_2$ as secondary phase (ICDD PDF4+ 96-100-0046). On the other hand, the diffraction pattern showing unsubstituted powder obtained using mussel shells demonstrated the synthesis of HAp (ICDD PDF4+ 96-900-2214) without any secondary phase, as presented in Table 2. Furthermore, all substituted samples presented in their diffraction data the successful HAp synthesis in agreement with the standard data. Additionally, for all the samples obtained from eggshells, we identified the sharp principal diffraction peaks at 2θ values of 25.82, 31.69, 46.71, and 49.42, which correspond to (0 0 2), (2 1 1), (2 2 2), and (2 1 3) Miller indices. Moreover, the samples obtained from mussel shells exhibited broader diffraction peaks. These peaks were emphasized at 2θ values of 25.81, 29.21, 31.99, 46.76, and 49.39 corresponding to (0 0 2), (2 1 0), (2 1 1), (2 2 2) and (2 1 3) Miller indices.

The increased similarity of XRD patterns between substituted and unsubstituted powders proved Mg^{2+} incorporation in the HAp lattice without affecting the chemical structure [13]. The incorporation of doping ions is also confirmed by the modification of lattice parameters of the obtained samples, as shown in Table 2.

Table 2

Phase content, crystallinity, crystallite size, and structural parameters of the synthesized samples, obtained by Rietveld Refinement.

Code	GOF	Phase content (%)		Crystallinity (%)	Average crystallite size (nm)	Lattice Parameters		
		HAp	$Ca(OH)_2$			Unit cell a (Å)	Unit cell c (Å)	Unit cell volume (Å^3)
HAp_C	2.657	92.2	7.8	50.6	34.46	9.429	6.880	529.762
HAp_Mg_1_C	2.874	100	-	51.45	21.68	9.426	6.881	529.551
HAp_Mg_3_C	2.746	100	-	51.61	22.68	9.423	6.876	528.806
HAp_Mg_5_C	2.916	100	-	49.89	27.04	9.425	6.875	529.015
HAp_S	3.069	100	-	49.92	35.49	9.395	6.918	528.933
HAp_Mg_1_S	3.23	100	-	52.70	25.59	9.424	6.877	529.012
HAp_Mg_3_S	3.065	100	-	51.58	20.33	9.423	6.876	528.865
HAp_Mg_5_S	2.834	100	-	49.54	21.68	9.426	6.874	528.999

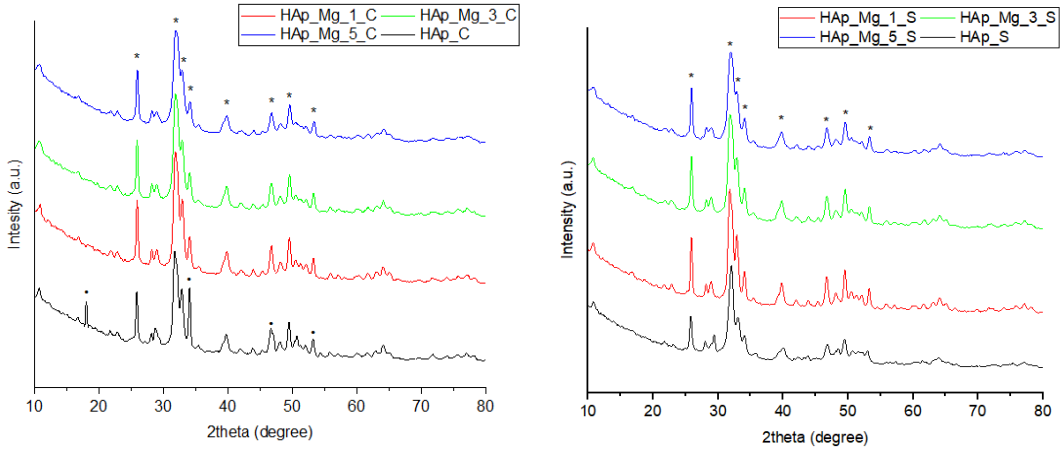

(a) (b)

•—$Ca(OH)_2$, *— $Ca_{10}(PO_4)_6(OH)_2$

Fig. 1. XRD patterns of the Mg-substituted HAp compared to the unsubstituted sample obtained from (a) eggshells and (b) mussel shells.

The lattice parameters (unit c, a, and unit cell volume) are influenced depending on the doping concentration. Researchers reported that Mg-substituted HAp alterations are influenced by the suppression of HAp crystal growth due to Mg ions. Mg^{2+} has an ionic radius of around 0.66 Å, while Ca^{2+} has an ionic radius of 0.99 Å. In this regard, Mg^{2+} can effortlessly replace Ca^{2+} ions in the HAp structure. All these lattice modifications are generated by the replacement between Mg and Ca ions, generating not only pattern deformation but also shape modifications [8]. Regarding the crystallinity and crystallite size of the HAp samples, the influence of

doping ions could also be observed. While the concentration of doping ions increases, the crystallinity increases, and average crystallite size decreases, also confirming the incorporation of doping ions into the HAp structure.

3.1.2. Scanning Electron Microscopy (SEM)

SEM analysis was performed to determine the morpho-structural characteristics of unsubstituted and Mg-substituted HAp powders. From Fig. 2, it could be observed the elongated shape of the particles, with dimensions between 5 nm to 22 nm. In addition, as the concentration of the doping ions was increased, the morphology of the particles was influenced.

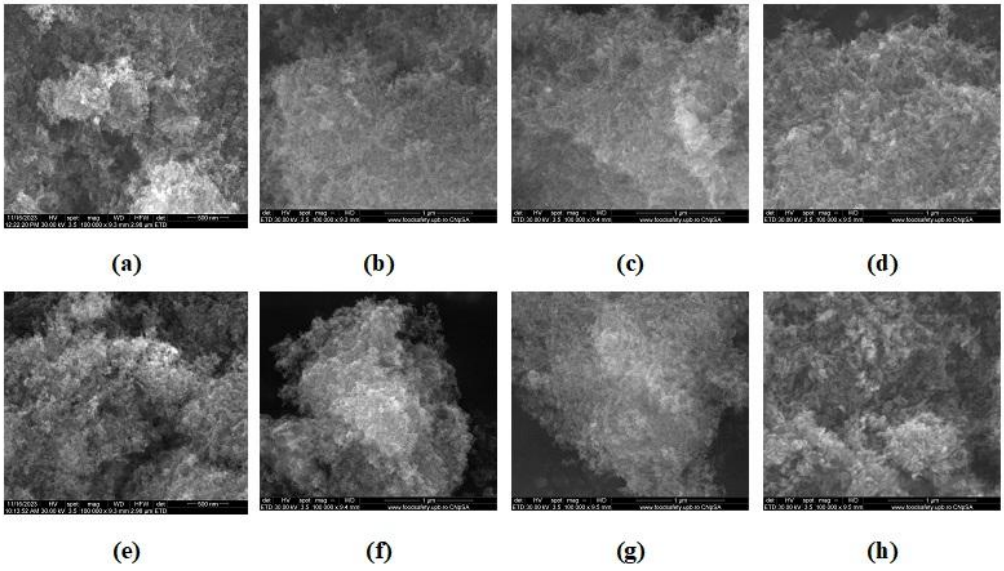

Fig. 2. SEM micrographs of obtained samples: (a) HAp_C, (b) HAp_Mg_1_C, (c) HAp_Mg_3_C, (d) HAp_Mg_5_C, (e) HAp_S, (f) HAp_Mg_1_S, (g) HAp_Mg_3_S, (h) HAp_Mg_5_S.

3.1.3. Fourier-Transform Infrared Spectroscopy (FT-IR)

In Fig. 3, the FT-IR spectra of the obtained samples are presented. By investigating the synthesized samples, the main functional groups that correspond to HAp could be identified: the bands of PO_4^{3-} groups (559-601 cm^{-1} and 962-1089 cm^{-1}), the υ3 vibration bands of CO_3^{2-} (1416-1541 cm^{-1}) and the OH groups (1614-1648 cm^{-1} and 3367-3567 cm^{-1}). Regarding the addition of doping ions, by increasing the concentration of Mg^{2+}, an increase in peak intensity could be observed. Furthermore, while PO_4^{3-} ion bands persist, the OH group bans broaden and decrease the number of hydroxyl groups. Additionally, the stretching vibration of OH at 3367-3567 cm^{-1} broadened, suggesting that the concentration of OH groups in the OH channel upon doping is not modified, while the presence of the

substituent in the adjoining area diminishes the vibration of a hydroxyl group [13-16].

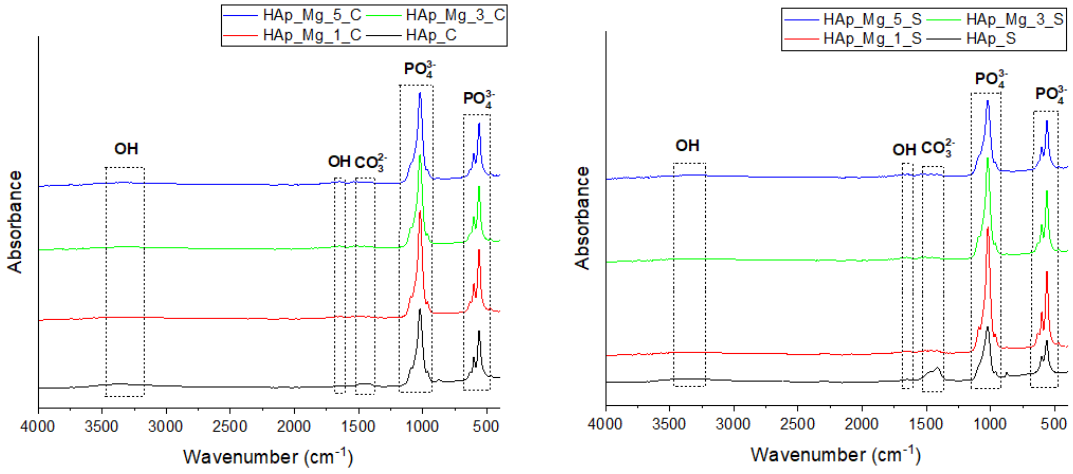

(a) (b)

Fig. 3. FTIR spectrum of the Mg-substituted HAp compared to the unsubstituted sample obtained from (a) eggshells and (b) mussel shells.

3.1.4. Biological Evaluation

The biological activity was evaluated by performing the XTT assay. In this experiment, MC3T3-E1 osteoblast cells were applied to determine the effects of substituted and unsubstituted samples considering their cellular viability, as shown in Fig. 4. All synthesized powders presented good cell viability after completing the *in vivo* experiments. Additionally, the incorporation of Mg^{2+} did not negatively affect the bioactivity compared to the control.

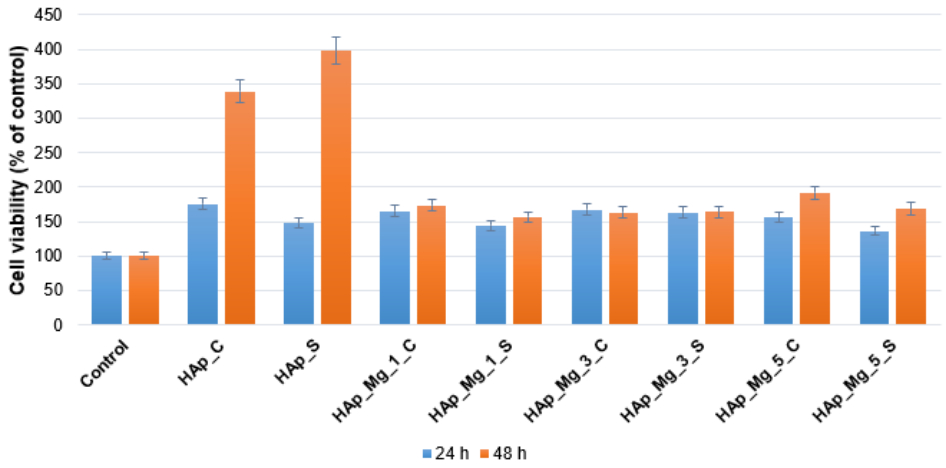

Fig. 4. Cell viability results of unsubstituted and Mg-substituted HAp samples. The bars represent the standard derivations of the absorbances obtained.

Further, an increase in cell viability was demonstrated after 48 h, demonstrating the suitability of the developed materials to be further applied in biomedical applications, thus enhancing osteoblast cell proliferation.

3.2. Discussion

This study demonstrated the successful synthesis of HAp using eggshells and mussel shells as CaO precursors. By combining the co-precipitation and microwave-assisted hydrothermal maturation process, the production of HAp powders with distinct characteristics was performed. The XRD analysis confirmed the successful synthesis of HAp from both biogenic sources, with eggshell-derived HAp exhibiting minor secondary phases, while mussel shell-derived HAp demonstrated higher purity. Another significant finding of the study was the successful incorporation of Mg^{2+} ions into the HAp lattice. Further, this incorporation led to lattice modifications, alteration of crystallinity and crystallite size of the samples. These modifications indicated the potential influence of the substituted ion concentration on the structural properties of HAp, offering the possibility to tailor the material's properties for specific applications. The morpho-structural characteristics of the HAp powders were further explored through SEM, revealing elongated particle shapes and size differences influenced by the concentration of doping ions. The morphological alterations emphasized the impact of Mg^{2+} substitution on particle properties, potentially affecting the material's performance in biological settings. Furthermore, FT-IR spectroscopy identified the main functional groups of HAp, with notable changes identified upon Mg^{2+} substitution. The variation in peak intensities and broadening of bands indicated structural modifications induced by the substituted ions, confirming the alteration in the chemical composition and incorporation within the HAp structure. The biological assessment using the XTT assay demonstrated robust cell viability, particularly in MC3T3-E1 osteoblast cells, highlighting the suitability of the synthesized HAp powders for biomedical applications. The incorporation of Mg^{2+} did not compromise the material's bioactivity and even led to improved cell viability over time, highlighting the potential for enhanced cellular responses with Mg^{2+} - substituted HAp.

6. Conclusions

In this study, unsubstituted and Mg-substituted HAp powders were synthesized through the co-precipitation method followed by the microwave-assisted hydrothermal maturation process. As CaO sources, eggshells and mussel shells were selected. With the aid of XRD, the successful synthesis of HAp was demonstrated. Further, Mg^{2+} incorporation into the HAp chemical structure was also confirmed. Considering doping ions concentration, it could be observed that while concentration increased, the peak intensity increased significantly, with a

slight peak shift of all major peaks. Additionally, through the Rietveld refinement, the modification of lattice parameters (unit c, a, and unit cell volume), crystallinity, and average crystallite size was observed, confirming the substitution into HAp. The morphological properties of the obtained samples were examined following SEM investigations. From the micrographs, it could be determined that the increase in dopant concentration led to shape alterations which may be due to the nanoparticles tendency to agglomerate. The influence of doping ions was also observed through FT-IR, confirming firstly the presence of HAp main functional groups. Moreover, doping ions incorporation did not affect the principal groups, while a minor decrease in peak intensity corresponding to the OH groups was shown. This modification was generated by the substitution of Ca^{2+} in the structure of HAp. Regarding the biological activity, all synthesized samples showed superior cellular viability, confirming their applicability in bone tissue engineering. These findings highlight the possibility for future investigations in tailoring HAp properties for biomedical applications, providing valuable insights into material design strategies that can enhance bioactivity and biocompatibility for purposes such as tissue engineering and regenerative medicine.

REFERENCES

[1]. *A. Mahanty, R. Kumar, D. Shikha, and S.K. Sinha*, "Synthesis and characterization of new biomaterial ZnMg doped HAp for orthopaedic implant" in Ceramics Internat., **vol. 49**, no. 17, Sept. 2023, pp. 28965-28973.

[2]. *A. Mahanty, and D. Shikha*, "Design of a new Ag/Mg/Zn alloyed doped hydroxyapatite hybrid biomaterial", in Mater. Chem. Phys., **vol. 311**, Jan. 2024, pp. 128553.

[3]. *S. Sebastiammal, A.S.L. Fathima, K.A. Al-Ghanim, M. Nicoletti, G. Baskar, J. Iyyappan, and M. Govindarajan, "*Synthesis and characterisation of magnesium-wrapped hydroxyapatite nanomaterials for biomedical applications", in Surf. Interfaces, **vol. 44**, Jan. 2024, pp. 103779.

[4]. *Ş. Ţălu, R.S. Matos, H.D. da F. Filho, D.Predoi, S.L. Iconaru, C.S. Ciobanu, and L. Ghegoiu*, "Morphological and fractal features of cancer cells anchored on composite layers based on magnesium-doped hydroxyapatite loaded in chitosan matrix", in Micron, **vol. 176**, Jan. 2024, pp. 103548.

[5]. *S. Helen, L. Saravanan, V. Sabari, K. Senthilkumar, and N. Kanagathara*, "Temperature-dependent dielectric investigation of dual-ions doped hydroxyapatite nanoparticles", in Inorg. Chem. Commun., **vol. 158**, no. 2, Dec. 2023, pp. 111606.

[6]. *C.R. Dumitrescu, I.A. Neacsu, V.A. Surdu, A.I. Nicoara, C.I. Codrea, C.E. Pop, R. Trusca, and E. Andronescu*, Maturation of hydroxyapatite from biogenic calcium source – a comparative study, in U.P.B. Sci. Bull., **vol. 84**, no. 1, Mar. 2022, pp. 19-30.

[7]. *G. Karunakaran, E.-B. Cho, G.S. Kumar, E. Kolesnikov, G. Janarthanan, M.M. Pillai, S. Rajendran, S. Boobalan, K.G. Sudha, M.P. Rajeshkumar*, "Mesoporous Mg-doped hydroxyapatite nanorods prepared from bio-waste blue mussel shells for implant applications", in Ceramics Internat., **vol. 46**, no.18, Dec. 2020, pp. 28514-28527.

[8]. *M.S.F. Hussin, H.Z. Abdullah, M.I. Idris, and M.A.A. Wahap*, "Extraction of natural hydroxyapatite for biomedical applications-A review", in Heliyon, **vol. 8**, no. 8, Aug 2022, pp. e10356.

[9]. *L.M. Cursaru, M. Iota, R.M. Piticescu, D. Tarnita, S.V. Savu, I.D. Savu, G. Dumitrescu, D. Popescu, R.-G. Hertzog, and M. Calin*, "Hydroxyapatite from Natural Sources for Medical Applications", in Materials, **vol. 15**, no.15, Jul. 2022, pp. 5091.

[10]. *W. Shi, M. Yi, Y. Liu, S. Huang, J. Fan, P.N.L. Lens, and B. Zhang*, "Preparation of hydroxyapatite (HAP) from waste eggshells for enhancing the granulation and treatment performance of aerobic granular sludge: Enhancement effects and mechanism insights", in J. Chem. Eng., **vol. 477**, Dec. 2023, pp. 147096.

[11]. *S. Liu, K. Yao, B. Wang, and M.-G. Ma*, "Microwave-assisted hydrothermal synthesis of cellulose/ZnO composites and its thermal transformation to ZnO/carbon composites". In Iran Polym J 26, **vol. 26**, Aug. 2017, pp. 681–691.

[12]. *F.E.-T. Heakal, O.S. Shehata, A.M. Bakry, and N.S. Tantawy*, "Influence of anodization and bovine serum albumin on the degradation of new AXJ-magnesium alloy system as a bioabsorbable orthopedic implant.", in J. Electroanal. Chem., **vol. 918**, Dec. 2022, pp. 116458.

[13]. *D.O. Obada, K.A. Salami, A.N. Oyedeji, O.O. Fasanya, M.U. Suleiman, B.A. Ibisola, A.Y. Atta, D. Dodoo-Arhin, L.S. Kuburi, M. Dauda, and E.T. Dauda*, "Solution combustion synthesis of strontium-doped hydroxyapatite: Effect of sintering and low compaction pressure on the mechanical properties and physiological stability". In Mater. Lett., Dec. 2021, **vol. 304**, pp. 130613.

[14]. *V.S. Bystrov, E.V. Paramonova, L.A. Avakyan, N.V. Eremina, S.V. Makarova, and N.V. Bulina*, "Effect of Magnesium Substitution on Structural Features and Properties of Hydroxyapatite", in Materials, **vol. 16**, Aug 2023, pp. 5945.

[15]. *A.R. Noviyanti, I. Rahayu, R.P. Fauzia, and Risdiana*, "The effect of Mg concentration to mechanical strength of hydroxyapatite derived from eggshell", Arab. J. Chem., vol. 14, no. 4, Apr. 2021, pp. 103032.

[16]. *A. Jenifer, K. Senthilarasan, S. Arumugam, P. Sivaprakash, S. Sagadevan, and P. Sakthivel*, "Investigation on antibacterial and hemolytic properties of magnesium-doped hydroxyapatite nanocomposite", Chem. Phys. Lett., vol. 771, May 2021, pp. 138539.